Influence of Stable Crack Propagation Characteristics on Fracture Toughness of Polycrystalline Ceramics

K. Mori[1], I. Torigoe[2] and T. Iwamoto[3]

[1] Kumamoto University, Faculty of Engineering, Department of Mechanical Engineering
2-39-1 Kurokami, Kumamoto, 860-8555 JAPAN
kmori@mech.kumamoto-u.ac.jp
[2] torigoe@kumamoto-u.ac.jp
[3] 020d8205@gsst.stud.kumamoto-u.ac.jp

ABSTRACT. *Characteristics of fracture toughness of polycrystalline ceramics are investigated by numerical simulations and indentation fracture test for polycrystalline alumina ceramics. Generally ceramics fracture from a defect. A crack propagates from the defect stably under monotone increasing load before catastrophic fracture. This stable crack propagation determines the characteristics of fracture toughness of ceramics. In this study we perform crack propagation simulations by using boundary element method. The relationship between the micro crack extension resistance and the macro fracture toughness in polycrystalline ceramics is investigated. According to the results, the crack extension area is wide and the standard deviation of the macro fracture toughness is large, so that the standard deviation of the micro crack extension resistance is large. It is worth noticing that the aforementioned results obtained in the present paper might be useful also when stable crack propagation due to fatigue loading is investigated.*

INTRODUCTION

When using ceramics as structural materials we have to grasp its statistic character of strength because the strength scatters widely. The reasons why it scatters widely are the dispersion of defect size and the dispersion of strength of materials surrounded the defect. The dispersion of defect size corresponds to the dispersion of the stress intensity factor and the dispersion of strength of materials corresponds to the dispersion of the fracture toughness.

In the present paper we propose a fracture model for stable crack propagation under static loading (although an extension of the present model to fatigue loading can be conjectured) in polycrystalline ceramics. Based on this model, the characteristics of fracture toughness are investigated by the numerical crack extension simulations. We also conduct indentation fracture tests to obtain the characteristics of the fracture toughness for polycrystalline ceramics.

FRACTURE MODEL IN POLYCRYSTALLINE CERAMICS

First, we consider the fracture criterion from a defect in polycrystalline ceramics.

Figure 1 shows a schematic diagram of a surface defect. It is assumed that the boundary of the defect is a crack front because a crack emanates from defects before catastrophic fracture in polycrystalline ceramics [1, 2].

The crack fronts are indented complicatedly and the stress intensity factors have distribution along the crack front. Let the stress intensity factors in the micro elements along the crack front be $k^*_{I,1}$, $k^*_{I,2}$, ... , $k^*_{I,m}$.

On the other hand, the crack extension resistances in the micro region also have distribution due to residual microstresses [3, 4]. Let the crack-extension resistances be $k^*_{C,1}$, $k^*_{C,2}$, ... , $k^*_{C,m}$.

We consider the fracture criterion of micro elements. Boundaries of elements mean pinning sites where crack stops. Namely, each element does not correspond to one grain directory.

One element fractures when the micro stress intensity factor, $k^*_{I,i}$ for the element reaches the micro crack extension resistance, $k^*_{C,i}$. However, crack stops due to the new elements with higher crack extension resistance, $k^*_{C,j}$, $k^*_{C,j+1}$ and $k^*_{C,j+2}$, because the crack extension resistance of the fractured element is one of the lowest values. The crack progresses stably by this repetition.

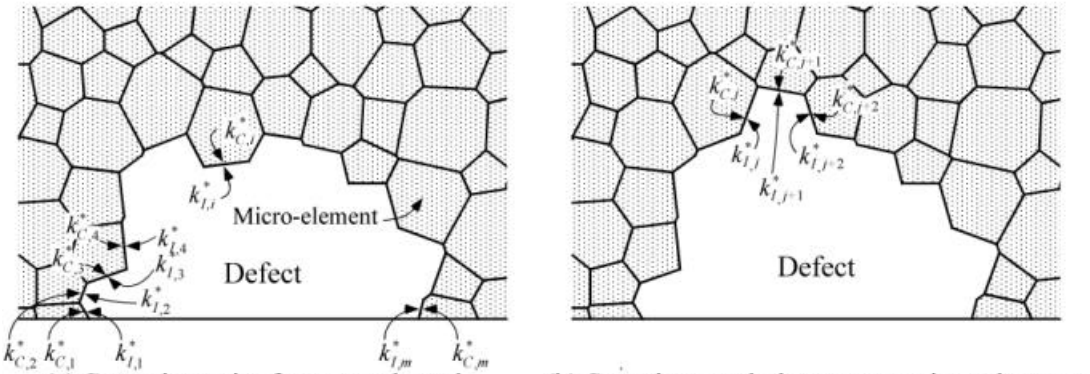

Figure 1. Fracture criterion of micro-element.

NUMERICAL SIMULATIONS

Based on the proposed fracture model, crack extension simulation is performed. We adopted the three dimensional boundary element method [5].

Figure 2 shows meshing of the initial defect. We assume that each micro element is a right hexagon. The shape of the initial defects is semi-penny shape. Each number of elements was assumed to be 11, 45 and 162.

The stress intensity factors, $k_{I,i}$ obtained by the boundary element method are deferent from the actual stress intensity factors, $k^*_{I,i}$, mentioned above because the shape of each micro element differs. Then we introduce new parameter for crack extension resistance, $k_{C,i}$ and the difference of the stress intensity factors are added to the value of $k_{C,i}$. Namely,

$$k_{C,i} = k^*_{C,i} + (k_{I,i} - k^*_{I,i}) \quad . \tag{1}$$

One example of distribution of crack extension resistance is shown in Fig. 3. The probability distribution of the micro crack extension resistance is assumed to be a normal distribution. Numerical simulation is performed for the standard deviation of the micro crack extension resistance, *SD* = 0.1, 0.2, 0.3 and 0.4.

Let the nominal stress, σ_n increase and make the crack extent from the initial defect. We assume that the element fracture when the micro stress intensity factor, $k_{I,i}$ reaches the micro crack extension resistance, $k_{C,i}$.

Figure 4 shows a crack extension process due to the increase of σ_n when n = 11 and *SD* = 0.4. The nominal stress is normalized by the fracture stress, σ_f':

$$\sigma_f' = K_C / 0.65\sqrt{\pi\sqrt{area}} \tag{2}$$

where $\sqrt{area}$ is the projected are of the initial defect [6], and the ratio of $\bar{k}_C / K_C$ is assumed to be 1.0.

In Fig. 4, it is shown that the values of σ_n / σ_f' at the fracture element number 1, 2, 5, 7 and 11 are higher than those of σ_n / σ_f' before the fracture element number. That is, the crack stops at the fracture element number, 1, 2, 5, 7 and 11. Each stop crack is shown in Fig. 5. The value of σ_n / σ_f' has the maximum value when the fracture element number is 11. This maximum value becomes the fracture strength of this material.

Figure 6 shows cracks just before catastrophic fracture when n = 162. From Fig. 6 we can see that the crack becomes a semi-ellipse when *SD* of the micro crack extension resistance is small and the crack extension region, which is identified by the fracture element number (*FEN*), becomes large, so that *SD* becomes large.

The values of the normalized macro fracture toughness, $K_C / \bar{k}_C$, are plotted on a normal probability paper as shown in Fig. 7. We can see that the values of $K_C / \bar{k}_C$ can be approximated by normal distribution.

The mean values, the standard deviations and the values of the coefficient of variation, *COV* are shown in Table 1. The root area in Table 1 is the projected area of the initial defect, where the area of micro fracture element is assumed to be one. We can see that the value of *COV* is large, so that the micro crack extension resistance *SD* is large.

(a) 11 element defect (n = 11)

(b) 45 element defect (n = 45)

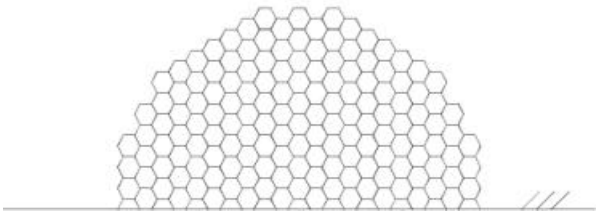

(c) 162 element defect (n = 162)

Figure 2. Initial defect meshes.

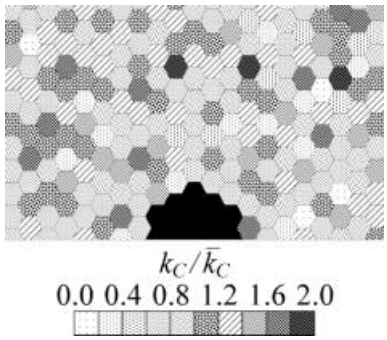

Figure 3. Distribution of crack extension resistance.

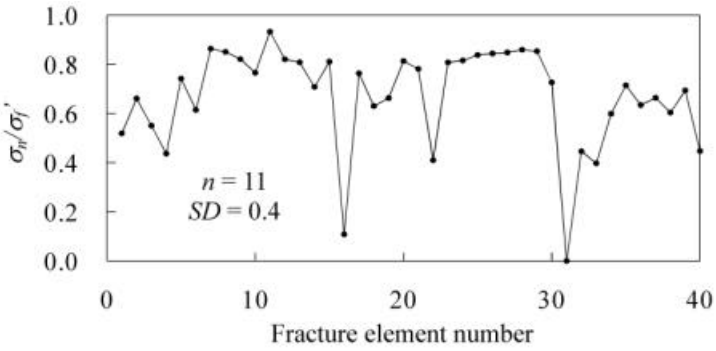

Figure 4. Crack extension (n = 11, SD = 0.4).

On the other hand, the difference of the fracture element number corresponds to the difference of the grain size when the defect sizes are assumed to be constant. Then the value of *COV* is large, so that the grain size is large.

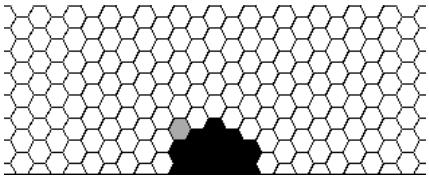

Fracture element number = 1

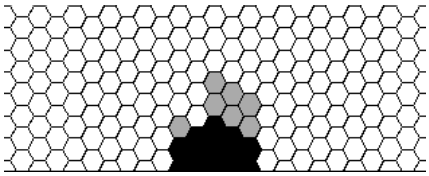

Fracture element number = 7

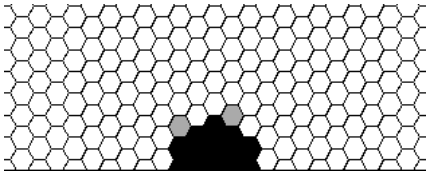

Fracture element number = 2

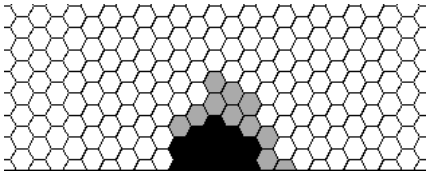

Fracture element number = 11
(Crack just before catastrophic fracture)

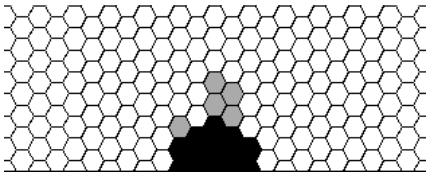

Fracture element number = 5

Figure 5. Crack extension process (n = 11, SD = 0.4).

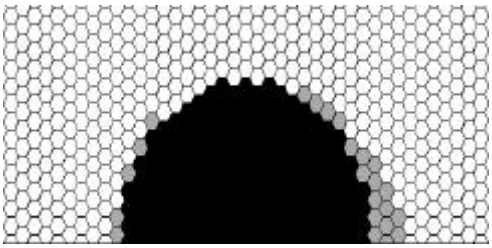

(a) SD = 0.1 (FEN = 23)

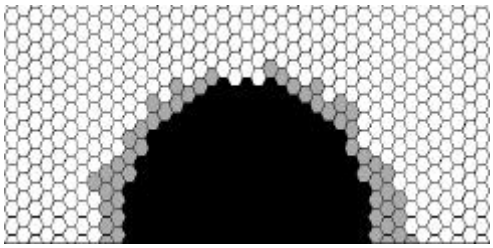

(c) SD = 0.3 (FEN = 52)

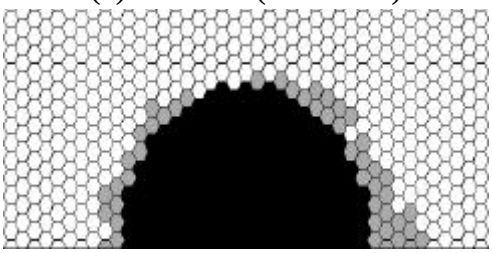

(b) SD = 0.2 (FEN = 47)

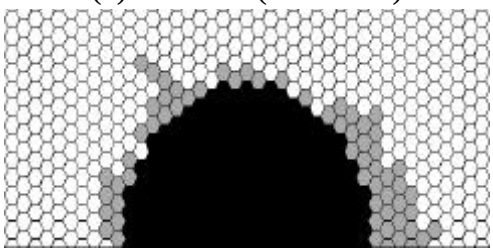

(d) SD = 0.4 (FEN = 62)

Figure 6. Cracks just before catastrophic fracture (n = 162).

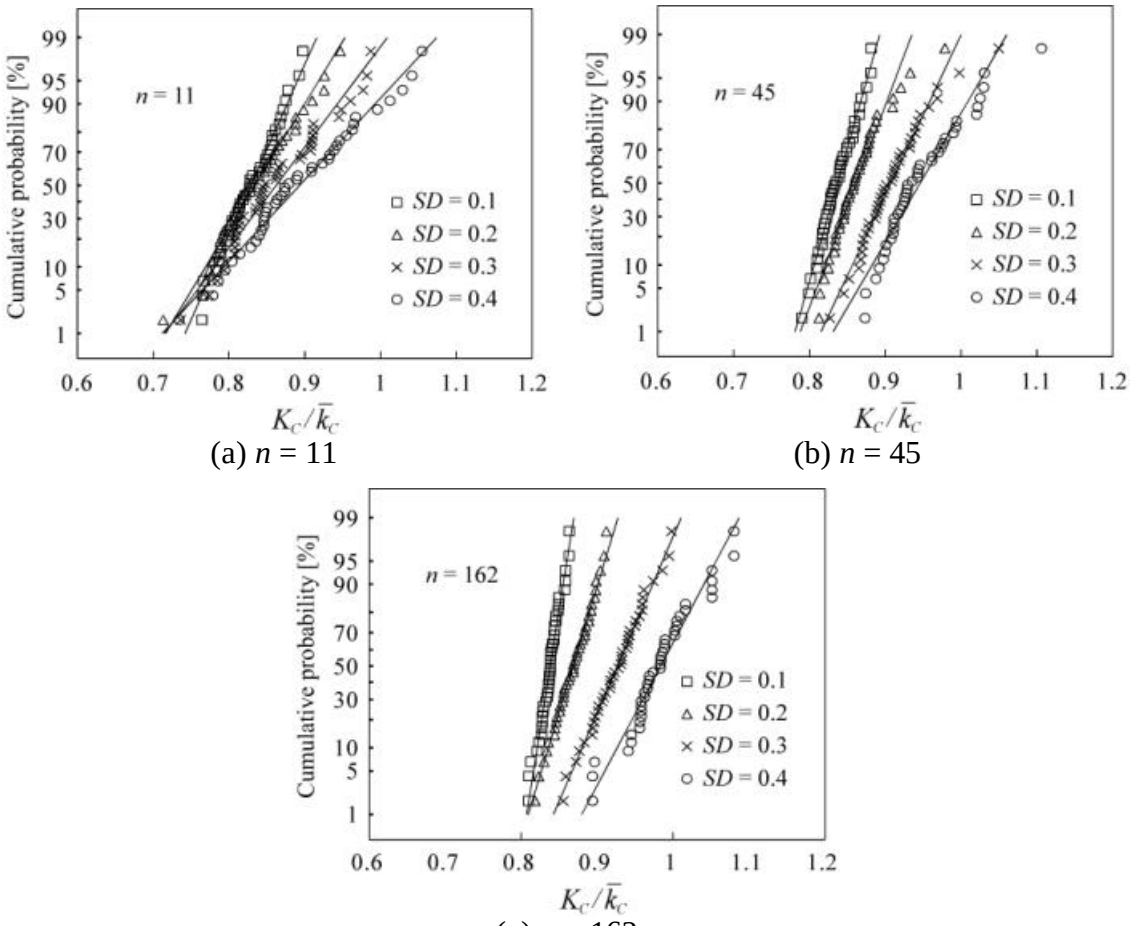

(a) n = 11 (b) n = 45

(c) n = 162

Figure 7. Normalized fracture toughness plotted in normal probability paper.

Table 1. Statistic characteristics of nondimensional fracture toughness.

Initial element number n	Mean root area $\sqrt{area}$	Standard deviation SD	Mean fracture toughness $\overline{K}_C/\overline{k}_C$	Standard deviation σ_{Kc}	Coefficient of variation COV
11	9.5	0.1	0.8288	0.03502	0.04225
		0.2	0.8342	0.05076	0.06084
		0.3	0.8619	0.06128	0.07109
		0.4	0.8929	0.07557	0.08464
45	42.5	0.1	0.8367	0.02280	0.02725
		0.2	0.8631	0.03386	0.03923
		0.3	0.9092	0.04277	0.04705
		0.4	0.9481	0.05093	0.05372
162	156.5	0.1	0.8380	0.01291	0.01540
		0.2	0.8681	0.02392	0.02755
		0.3	0.9265	0.03455	0.03729
		0.4	0.9835	0.04413	0.04487

EXPERIMENTS

Here we compare the numerical results with experimental data for alumina ceramics in order to check the numerical results.

Figure 8 shows fracture toughness for alumina ceramics plotted on the normal probability paper. Indentation fracture method was used to measure the fracture toughness.

The mechanical properties of the alumina ceramics are shown in Table 2. The crack size and fracture properties are shown in Table 3.

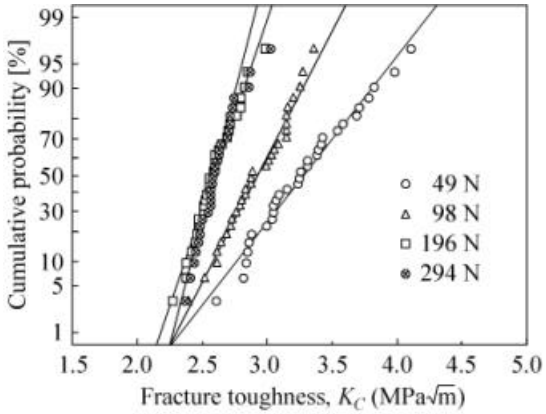

Figure 8. Fracture toughness, K_C for alumina ceramics.

Table 2. Mechanical properties of alumina ceramics.

Mean bending strength σ_{4B} [MPa]	Vickers hardness number H_v	Fracture toughness (SEPB) K_{IC} [MPa$\sqrt{m}$]	Young's modulus E [GPa]	Poisson's ratio ν	Mean grain size $\overline{d}$ [μm]
300	1480	3.2	380	0.2	3.6

Table 3. Crack size and fracture properties.

Indentation load P [N]	Mean half crack length $\overline{c}$ [μm]	Mean root area $\sqrt{area}$ [μm]	Mean fracture toughness $\overline{K}_C$ [MPa$\sqrt{m}$]	Standard deviation σ_{Kc} [MPa$\sqrt{m}$]	Coefficient of variation [-]
49	113	149	3.28	0.367	0.112
98	190	243	2.92	0.242	0.0829
196	329	406	2.60	0.158	0.0608
294	431	526	2.61	0.143	0.0548

Here we compare the numerical results and the experimental results. Figure 9 shows the coefficient of variation, *COV*, for the fracture toughness of the numerical simulation in Table 1. Let us put the root of the projected defect area in the abscissa, where the area

of one fracture element is assumed to be one. The values of *COV* can be approximated with an involution function as shown in Fig. 9.

Figure 10 shows coefficient of variation, *COV*, for the fracture toughness of the alumina ceramics in Table 3. The values of *COV* can also be approximated with an involution function.

The exponent of the approximate expression for *COV* in the experimental results is close to that for *COV* in the numerical simulation when *SD* = 0.2. Namely, if fracture elements in alumina are much larger than one grain size, the value of *COV* in the numerical simulation and that in the experimental results coincides with each other.

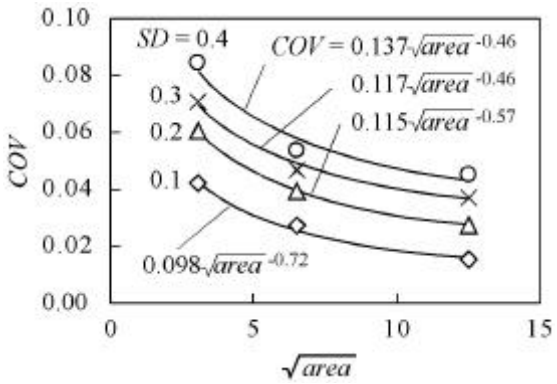

Figure 9. *COV* for the fracture toughness in the numerical results.

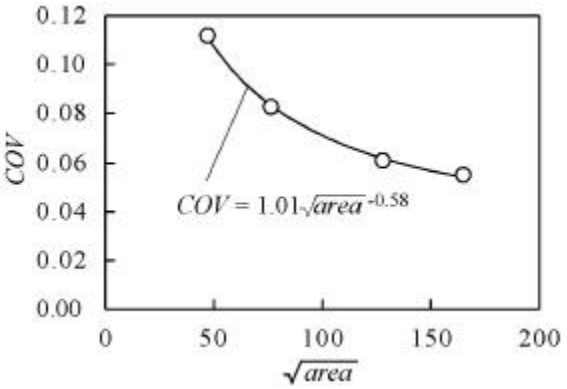

Figure 10. *COV* for fracture toughness in the experimental results.

CONCLUSIONS

We propose a fracture model for stable crack propagation under static loading (although an extension of the present model to fatigue loading can be conjectured) in polycrystalline ceramics. Based on the model we have performed the numerical simulations of fracture for polycrystalline ceramics. Experiments of indentation fracture test for polycrystalline alumina were also performed.

1. The quantity of crack extension from an initial defect is large, so that the standard deviation of the micro crack extension resistance is large in the numerical simulation.
2. The coefficient of variation, *COV* for the fracture toughness is large, so that defect is small in the results of the numerical simulation and the experiment.
3. The value of *COV* for the fracture toughness in the results of the numerical simulation and the experiment can be approximated with an involution function. The exponent of the approximating expression for *COV* in the experiment results is close to that for *COV* in the numerical simulation when the standard deviation of the micro crack extension resistance, *SD* = 0.2.

ACNOWLEDGEMENTS

Thanks are due to Professor Noguchi H., Kyushu University for offering the program source to calculate stress intensity factor for arbitrary shape cracks.

REFERENCES

1. Ueno, A., Kishimoto, H., Kondo, T., Hosokawa, Y. and Morita, K (1996) *J. Soc. Mat. Sci. Jpn.* **45**, 1090-1096.
2. Mori, K., Noguchi, H. and Tabarrok, B. (1994) *J. Jpn. Soc. Mech. Eng.* **A-60**, 984-992.
3. Evans, A. G. (1978) *Acta Metall*. **26**, 1845-1854.
4. Ortiz, M. and Suresh, J. (1993) *J. Appl. Mech.*, **60**, 70-81.
5. Noguchi, H., Isida, M., Tsuru, H. and Mori, K. (1993) Boundary Element Methods. *Proceedings of 5th Japan and China Symposium on Boundary Element Method*, pp. 149-158, Elsevier, Tokyo.
6. Murakami, Y. and Isida, M. (1985) *J. Jpn. Soc. Mech. Eng.* **A-51**-461, 1050-1056.